Signatures of sub-GeV dark matter beams at neutrino experiments

Patrick deNiverville,[*] David McKeen,[†] and Adam Ritz[‡]

Department of Physics and Astronomy, University of Victoria, Victoria, British Columbia V8P 5C2, Canada
(Received 22 May 2012; published 29 August 2012)

We study the high-luminosity fixed-target neutrino experiments at MiniBooNE, MINOS and T2K and analyze their sensitivity to light stable states, focusing on MeV–GeV scale dark matter. Thermal relic dark matter scenarios in the sub-GeV mass range require the presence of light mediators, whose coupling to the Standard Model facilitates annihilation in the early universe and allows for the correct thermal relic abundance. The mediators in turn provide a production channel for dark matter at colliders or fixed targets, and as a consequence the neutrino beams generated at fixed targets may contain an additional beam of light dark matter. The signatures of this beam include elastic scattering off electrons or nucleons in the (near-)detector, which closely mimics the neutral current scattering of neutrinos. We determine the event rate at modern fixed target facilities and the ensuing sensitivity to sub-GeV dark matter.

I. INTRODUCTION

The existing gravitational evidence for dark matter provides limited information about its nongravitational interactions, and many candidates are sufficiently nonrelativistic and weakly interacting. The paradigm of a weak-scale thermal relic has the virtue of simplicity, with an abundance fixed without detailed knowledge of early-universe physics. However, direct detection experiments now impose stringent constraints on dark matter with a weak-scale mass; for example, spin-independent cross sections on nucleons must be at or below 10^{-45} cm^2. With this sensitivity now crossing the Higgs-mediation threshold, the minimal weakly interacting massive particle (WIMP) paradigm may need generalization to allow new interaction channels, beyond the electroweak sector of the standard model (SM). This would position dark matter as part of a more complex hidden sector containing additional light states. The required relic density could then be achieved without either weak-scale interactions or a weak-scale mass [1–4].

This viewpoint has some interesting implications when one looks at the existing limits on direct WIMP scattering. The sensitivity of direct-detection experiments tends to fall rather sharply for masses below a few GeV, due to the recoil energy detection threshold. The GeV mass scale also happens to coincide with the Lee-Weinberg bound [5], below which a thermal relic needs non-SM annihilation channels through light states to ensure the correct relic abundance. In combination, these observations naturally lead us to explore the use of new experimental tools to probe the sub-GeV mass range for thermal relic dark matter. The presence of light mediators coupled to the SM opens up the possibility of producing these states directly in accelerators or fixed target facilities. This

'dark force' phenomenology has been the focus of considerable interest in recent years. For example, a number of search strategies are based on the production of a GeV-scale vector mediator, with its subsequent decay to lepton pairs [2,6–11]. However, these search strategies are limited if, instead, the mediator is not the lightest hidden sector state and decays predominantly into the hidden sector, e.g., to dark matter. In this case, the scattering of those light states in a detector spatially separated from the production point represents perhaps the most efficient search strategy. Moreover, owing to the potentially large production rate, and the existence of large volume (near-)detectors, proton fixed-target facilities focusing on neutrino physics appear to be an ideal means for exploring these scenarios.

In this paper, we analyze the sensitivity of neutrino facilities to a boosted light dark matter beam produced via the generation and subsequent decay of GeV-scale mediators. This extends our earlier analysis of MeV-scale dark matter [11,12] to the full sub-GeV range. We will find that high-luminosity experiments such as MiniBooNE, MINOS and T2K have significant sensitivity to neutral current-like scattering of sub-GeV dark matter off nuclei in the (near-)detector. Although there is a long history of searches for exotics using fixed target facilities (see, e.g., Refs. [2,6–11,13]), neutrino experiments have the advantage that the large detector volume is sensitive to scattering signatures in addition to the products of SM decays. Since the recoil energy of sub-GeV halo dark matter is generally below threshold for underground direct detection experiments, and search channels at high-energy colliders are less sensitive in the case of light mediators, high-luminosity fixed-target experiments can play a complementary role in direct searches for dark matter.

In order to be as model-independent as possible, we parametrize the mediator interactions via the lowest dimension operators (portals) for a SM-neutral hidden sector, $\mathcal{L}_{int} = \sum \mathcal{O}_{SM}\mathcal{O}_{HS}$, where $\mathcal{O}$ denotes SM and hidden sector (HS) operators. For light dark matter, fixed-target

---
[*]pgdeniv@uvic.ca
[†]mckeen@uvic.ca
[‡]aritz@uvic.ca

facilities have an advantage if the mediator can be produced on-shell, so we focus on the renormalizable *vector* [14] and *scalar* SM portals [15]:

$$\mathcal{L}_{\text{int}} = \mathcal{L}_{\text{hid}}(X, \chi) + \begin{cases} \kappa F^Y_{\mu\nu} V^{\mu\nu}, & \text{vector portal} \\ A S H^\dagger H, & \text{scalar portal} \end{cases}, \quad (1)$$

where $F^Y_{\mu\nu}$ and H are the hypercharge field strength and the Higgs doublet, while $\mathcal{L}_{\text{hid}}$ provides hidden sector couplings between the mediator field $X = V^\mu$ or S and the light dark matter candidate χ. We will limit attention to the kinematic regime

$$m_X > 2m_\chi \sim \mathcal{O}(\text{MeV–GeV}), \quad (2)$$

so that with small portal couplings to the SM, the mediators predominantly decay into the hidden sector, $\text{Br}(X \to \chi\chi) \sim 1$.

The rest of this paper is organized as follows. In Sec. II, we describe our model for production of the dark matter beam at MINOS, T2K and MiniBooNE using both vector and scalar portals. In Sec. III, we discuss a number of existing constraints on sub-GeV dark matter, coupled to the SM via these portals, detail the annihilation and scattering rates, and determine viable models which can be probed using neutrino facilities. In Sec. IV, we focus on the most viable dark matter scenario, with scalar dark matter coupled via the vector portal, and analyze the sensitivity to the ensuing dark matter beam at MINOS, T2K and MiniBooNE. We conclude in Sec. V.

II. PRODUCTION OF THE DARK MATTER BEAM

A. DM interactions

The viability of thermal relic dark matter with a mass in the MeV–GeV range, well below the Lee-Weinberg bound, seemingly rests on the presence of a light hidden sector with states that can mediate annihilation [2–4]. Moreover, various phenomenological constraints [4] suggest that the most viable scenarios are those in which the hidden sector is uncharged under standard model symmetries. This naturally leads us to the portal interactions (1) as the primary means of probing these sectors at low energies.

To keep our analysis as general as possible, we will consider both the vector and Higgs portals for production of the dark matter beam in this section. These light mediators are necessary to allow for a viable annihilation channel in the early Universe, but we will be agnostic about the precise choice of model. This will allow us to analyze the raw sensitivity of neutrino facilities to production of these light states, and we will turn to the model-dependent constraints on viable light dark matter scenarios in the following sections.

To fix the interactions, we use the simplest realizations for the vector and scalar portals, and moreover we will only

need their low-energy manifestations. For the vector portal coupling, $F^Y_{\mu\nu} V^{\mu\nu}$, we have

$$\mathcal{L}_V = V_\mu (e\kappa J^\mu_{\text{em}} + e' J^\mu_\chi) + \mathcal{L}_{\text{kin}}(V, \chi) + \cdots, \quad (3)$$

where we have used $\partial_\mu F^{\mu\nu} = e J^\nu_{\text{em}}$ in terms of the electromagnetic current $J^\mu_{\text{em}} = \bar{q}\gamma^\mu q + \cdots$, while J^μ_χ is the corresponding U(1) current for scalar (or Dirac fermion) dark matter, with gauge coupling e',

$$J^\mu_\chi = \begin{cases} i\chi^\dagger \overset{\leftrightarrow}{\partial}^\mu \chi + \mathcal{O}(V^\mu), & \text{scalar} \\ i\bar{\chi}\gamma^\mu\chi, & \text{fermion} \end{cases}. \quad (4)$$

$\mathcal{L}_{\text{kin}}(V, \chi)$ contains canonical kinetic and mass terms for V and χ, and higher-order potential terms have not been written explicitly.

For the trilinear scalar portal coupling, $SH^\dagger H$, we have

$$\mathcal{L}_S = S(\theta J^m_{\text{EWSB}} + \beta J^m_\chi) + \mathcal{L}_{\text{kin}}(S, \chi) + \cdots, \quad (5)$$

where we have integrated out the SM Higgs, which induces a coupling $\theta \sim Av/m_h^2$ between S and the SM fermions via $J^m_{\text{EWSB}} = m_q\bar{q}q/v + \cdots$, while J^m_χ is an analogous mass current for scalar (or fermion) dark matter,

$$J^m_\chi = \begin{cases} m_\chi \chi^\dagger \chi, & \text{scalar} \\ i\bar{\chi}\chi, & \text{fermion} \end{cases}. \quad (6)$$

We have inserted a factor of m_χ in the scalar case, so that β remains a dimensionless coupling. As above, $\mathcal{L}_{\text{kin}}(V, \chi)$ contains the kinetic and mass terms for S and scalar/fermion dark matter χ.

We will refer to the mediator V or S generically as X, and the crucial kinematic assumption will be that $m_X > 2m_\chi$, so that the mediator can decay on-shell to dark matter. For small mixing via the portals, the hidden sector branching $\text{Br}(X \to \chi\chi) \sim 1$.

B. Production mechanisms

There are two viable production mechanisms for the mediator X at proton fixed-target experiments:

(i) *Direct production.*—This corresponds to hadron-level processes such as $pp(n) \to X^* \to \bar{\chi}\chi$ (or $\chi^\dagger\chi$) as shown in Figs. 1 and 2. In practice, since X can decay to $\bar{\chi}\chi$, we will use the narrow width approximation so that X is produced on-shell. In this approximation, valid to $\mathcal{O}(e'^2, \beta^2)$, the cross section for the production of a DM pair can be written as

$$\sigma(pp(n) \to X^* \to \bar{\chi}\chi) = \sigma(pp(n) \to X)\,\text{Br}(X \to \bar{\chi}\chi). \quad (7)$$

The direct production cross section of a vector mediator is
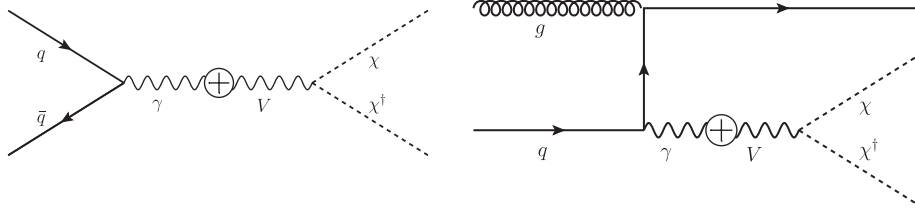
FIG. 1.   Direct production of scalar dark matter via the vector portal. The leading-order process is shown on the left, which is helicity suppressed in the forward direction. The process on the right is higher order in α_s, and also phase space suppressed, but has less helicity suppression in the forward direction.

$$\sigma(pp(n) \to V) = \int_\tau^1 dx \frac{d\sigma(pp(n) \to V)}{dx} = \frac{4\pi^2\alpha\kappa^2}{m_V^2}\sum_q e_q^2 \int_\tau^1 \frac{dx}{x}\tau\left[f_{q/p}(x)f_{\bar{q}/p(n)}\left(\frac{\tau}{x}\right) + f_{\bar{q}/p}(x)f_{q/p(n)}\left(\frac{\tau}{x}\right)\right], \qquad (8)$$

where e_q is the charge of quark q in units of the positron electric charge, $\tau = m_V^2/s$, and $\sqrt{s}$ is the hadron-level center-of-mass energy. The parton distribution function (PDF) $f_{q/p(n)}(x)$ gives the probability of extracting the quark q with momentum fraction x from a proton (neutron) and similarly for $f_{\bar{q}/p(n)}(x)$. We have omitted the scale, Q, at which the PDFs are evaluated. To obtain estimates, we use CTEQ6.6 PDFs [16] and set $Q = m_V$; varying Q in between $m_V/2$ and $2m_V$ resulted in an uncertainty in the production cross section of less than ~30% for $m_V > 1$ GeV at T2K and MINOS beam energies. Higher-order QCD corrections are large, introducing an error that can potentially be $\mathcal{O}(1)$.

The production cross section as a function of the DM lab frame energy, E_χ, and the angle between its lab frame momentum and the beam direction, θ, can be related to the differential cross section in Eq. (8) through

$$\frac{d\sigma(pp(n) \to V \to \bar{\chi}\chi)}{dE_\chi d\cos\theta}$$
$$= \left[\frac{\partial(x, \cos\hat{\theta})}{\partial(E_\chi, \cos\theta)}\right]\frac{d\sigma(pp(n) \to V)}{dx}$$
$$\times \mathrm{Br}(V \to \bar{\chi}\chi)g(\cos\hat{\theta}), \qquad (9)$$

where $\hat{\theta}$ is the angle between the momentum of χ and the beam in the V rest frame and the quantity in square brackets is the Jacobian associated with this variable change. The function g describes the angular
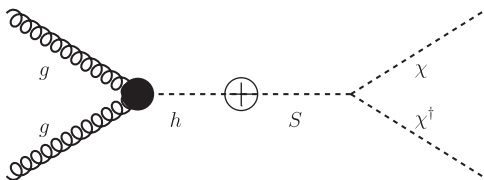
FIG. 2.   Direct production of dark matter via the scalar portal. The solid gluon fusion ggh vertex is generated at 1-loop.

distribution of the DM in the V rest frame. For scalar DM produced through a vector mediator, this is

$$g(\cos\hat{\theta}) = \frac{3}{4}(1 - \cos^2\hat{\theta}). \qquad (10)$$

If, instead, χ is a Dirac fermion, then

$$g(\cos\hat{\theta}) = \frac{3}{8}(1 + \cos^2\hat{\theta}). \qquad (11)$$

We will find the distribution of V momenta useful,

$$f_V(p_V) = \frac{1}{\sigma(pp(n) \to V)}\frac{d\sigma(pp(n) \to V)}{dp_V}$$
$$= \frac{1}{\sigma(pp(n) \to V)}\frac{dx}{dp_V}\frac{d\sigma(pp(n) \to V)}{dx}, \qquad (12)$$

with p_V the momentum of V in the lab frame which is related to x through

$$p_V = \frac{\gamma p_B m_T}{\sqrt{s}} \times \left[1 + \beta\left(1 + \frac{m_V^2 s}{(x - \tau/x)^2 p_B^2 m_T^2}\right)^{1/2}\right], \qquad (13)$$

where $m_T = m_{p,n}$ is the target mass, p_B is the momentum of the beam, $\gamma\beta = p_B/\sqrt{s}$, and $\gamma = 1/\sqrt{1 - \beta^2}$.

For illustration, in Figs. 3–5 we present the resulting direct production distributions for a vector mediator that subsequently decays to scalar DM at the T2K and MINOS experiments, where $E_{\mathrm{beam}} = 30$, 120 GeV ($\sqrt{s} \simeq 7.6$, 15.1 GeV), respectively; see Sec. IV for further details of these experiments. Figure 3 shows the total production cross section for pp and pn collisions at T2K and MINOS as a function of the vector mediator mass. After integrating over energy, the angular distribution of scalar DM is shown in the top of Fig. 4 at T2K ND280 and MINOS in the case that $m_V = 1$ GeV and $m_\chi = 300$ MeV. We focus on the off-axis ND280 detector at T2K, to contrast with the on-axis detector at MINOS in sampling the angular production distribution. However, comparing ND280 to the on-axis INGRID detector at T2K would provide a similar contrast. In the bottom left of Fig. 4, we zoom in
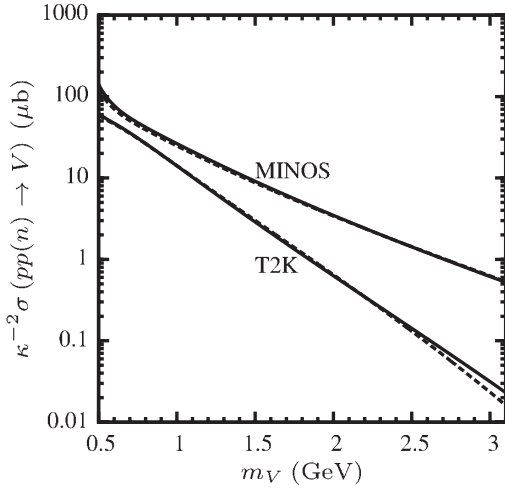
FIG. 3. The total production cross section of a vector mediator at T2K and MINOS energies as a function of the mediator mass. The solid and dashed curves indicate the cross sections for $pp \to V$ and $pn \to V$, respectively. The PDF scale has been fixed to $Q = m_V$.

on the relevant angular region for the off-axis T2K ND280 near detector and show the scalar DM angular distribution for $m_V = 1$ GeV and several DM masses produced in pp collisions. We do the same in the range of angles around the MINOS near detector in the bottom right of Fig. 4. As the mass of the DM is increased, it is produced in the more forward direction since its velocity in the V rest frame decreases. However, the angular distribution of scalar DM produced via a vector mediator, Eq. (10), suppresses the production of DM along the beam direction itself. Thus, despite the smaller cross section for the production of vector mediators as a result of the lower energy of its beam, a larger number of DM particles may pass through the off-axis T2K ND280 near detector than the on-axis MINOS near detector. This suppression along the beam axis is lessened somewhat when considering higher-order production mechanisms like the diagram on the right of Fig. 1, which we do not include in this study.

We show the energy distribution of scalar DM for $m_V = 1$ GeV and a range of m_χ in pp collisions for T2K at $\theta = 2°$ and for MINOS at $\theta = 0.025°$ in Fig. 5.
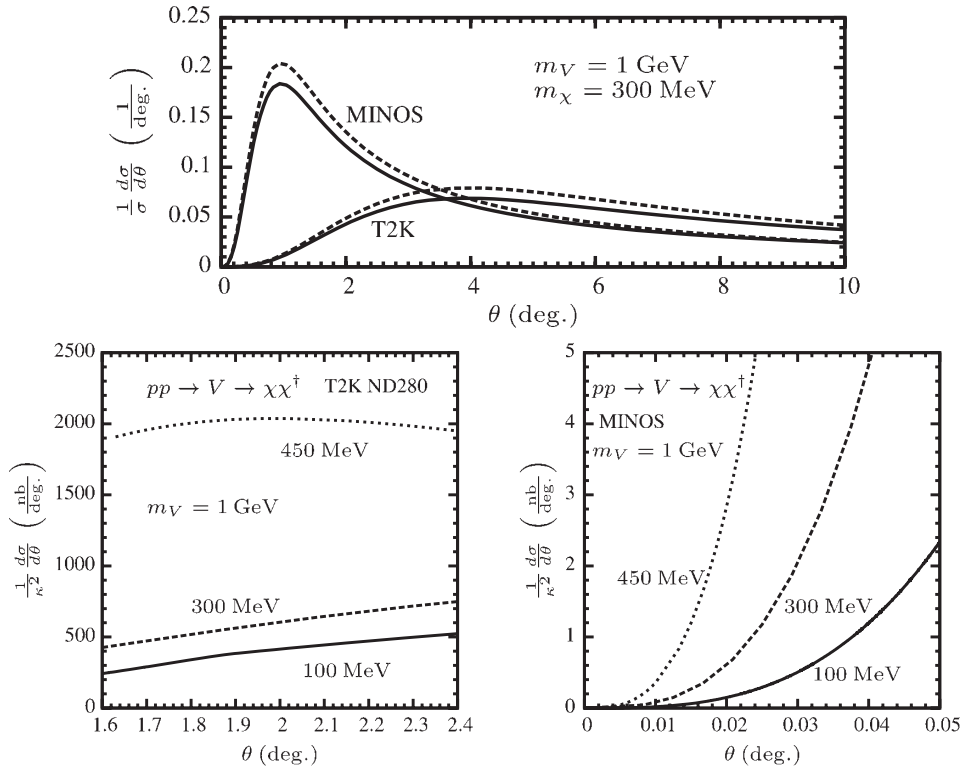
FIG. 4. Top: production distributions of scalar DM as a function of lab frame angle with respect to the beam, normalized to unity, in the case of a vector mediator with $m_V = 1$ GeV. The solid curves indicate pp collisions and the dashed ones pn collisions. The set of curves that peak at $\theta \sim 1°$ corresponds to a p beam with an energy equal to that of the MINOS experiment ($E_{\text{beam}} = 120$ GeV, $\sqrt{s} = 15$ GeV) while the curves that peak at $\theta \sim 4°$ correspond to a p beam with an energy equal to that of T2K ND280 ($E_{\text{beam}} = 30$ GeV, $\sqrt{s} = 7.6$ GeV). Bottom left: production cross sections in the case of a vector mediator ($m_V = 1$ GeV) and scalar DM for $m_\chi = 100, 300, 450$ MeV (solid, dashed, dotted) as functions of the DM angle with the beam in the lab frame in the case of pp collisions at an energy corresponding to the T2K experiment. The range of angles shown coincides with those covered by the off-axis ND280 near detector at T2K. Bottom right: the same at MINOS beam energy. The angles shown here are those that the MINOS near detector covers.
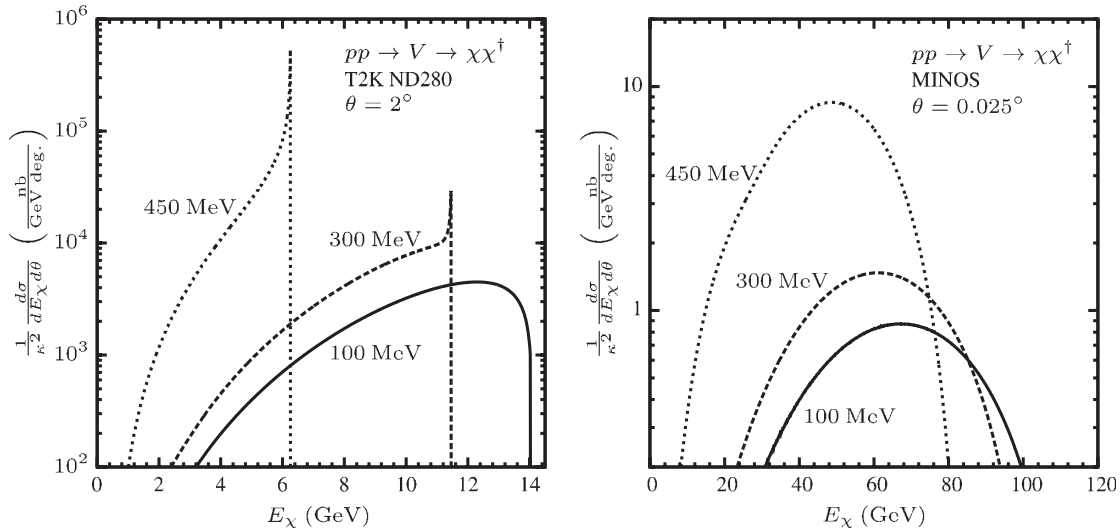
FIG. 5.   Left panel: $d\sigma(pp \rightarrow V \rightarrow \chi\chi^{\dagger})/dE_{\chi}d\theta$ in the case of scalar χ and vector V for $m_V = 1$ GeV and $m_{\chi} = 100, 300,$ 450 MeV (solid, dashed, dotted) for pp collisions at T2K ND280 at $\theta = 2°$. The cusps at the kinematic limits for larger m_{χ} are the result of a degeneracy in the angle between χ and the beam direction in the lab frame, θ, as a function of its value in the V rest frame, $\hat{\theta}$, for relatively small DM velocities (e.g., in the limit that the DM is produced at threshold, $\theta = 0$ for all $\hat{\theta}$). Right panel: the same for pp collisions at MINOS at $\theta = 0.025°$.

For a scalar mediator, the leading-order direct production cross section is

$$\sigma(pp(n) \rightarrow S) = \frac{\alpha_s^2 G_F N^2 \theta^2}{288\sqrt{2}\pi} \times \sum_q \int_{\tau}^{1} \frac{dx}{x} \tau f_g(x) f_g\left(\frac{\tau}{x}\right).$$

(14)

Here, $\tau = m_S^2/s$ and the PDF $f_g(x)$ is the probability of finding a gluon with momentum fraction x in a nucleon. Up to threshold effect corrections, N counts the number of quarks with a mass greater than $\sim 0.2 m_S$ [17].

The DM distributions in the lab frame can be related to the differential production cross section in the same way as in the vector mediator case in Eq. (9). In the S rest frame, the DM is simply produced isotropically,

$$g(\cos\hat{\theta}) = \frac{1}{2}.$$

(15)

Because of the weak scale and loop factor suppressions in Eq. (14), scalar mediator production is extremely small compared to the that of a vector at GeV scales. Thus, current neutrino experiments are much less sensitive to DM scenarios involving a GeV-scale spin-0 mediator than they are to a spin-1 mediator. Along with other factors to be discussed in the next section, this will lead us to focus only on the direct production of vector mediators.

(ii) *Indirect production.*—This corresponds to production of X via the decay of hadronic states (generically denoted ϕ) produced in the primary pp and pn interactions,

$$p + p(n) \rightarrow \phi + \cdots$$
$$\searrow X + \cdots$$
$$\searrow \chi\chi \quad (16)$$
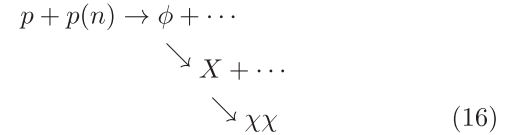
Depending on the beam energy and form of the target, the relevant decay lengths ensure that this entire sequence of events will occur either inside the target itself or in the subsequent decay volume.

In practice, this process is most important in the low mass range where, for example, the large production rate of neutral pseudoscalar mesons $\phi = \pi^0, \eta$ can dominate the overall production of V's in particular. The meson production distribution at MiniBooNE is well-described by the Sanford and Wang fit $f^{SW}(\theta, p)$ as described in Ref. [18], and utilized previously in Ref. [12]. To estimate the meson production distribution for MINOS and T2K, we make use of an analytic fit $f^{BMPT}(\theta, p)$ [19] to data for (averaged π^+ and π^-) pion production obtained over a range of energies, which can be scaled to cover the target materials for the experiments of interest. Example distributions for MINOS and T2K configurations are shown in Fig. 6. We have also tested this distribution against existing data published by NA61 [20] for the T2K target configuration, and found good agreement. The aforementioned NA61 data is used to estimate the total pion flux at T2K. As there is currently no equivalent pion production data set for MINOS, the pion production cross section was estimated by
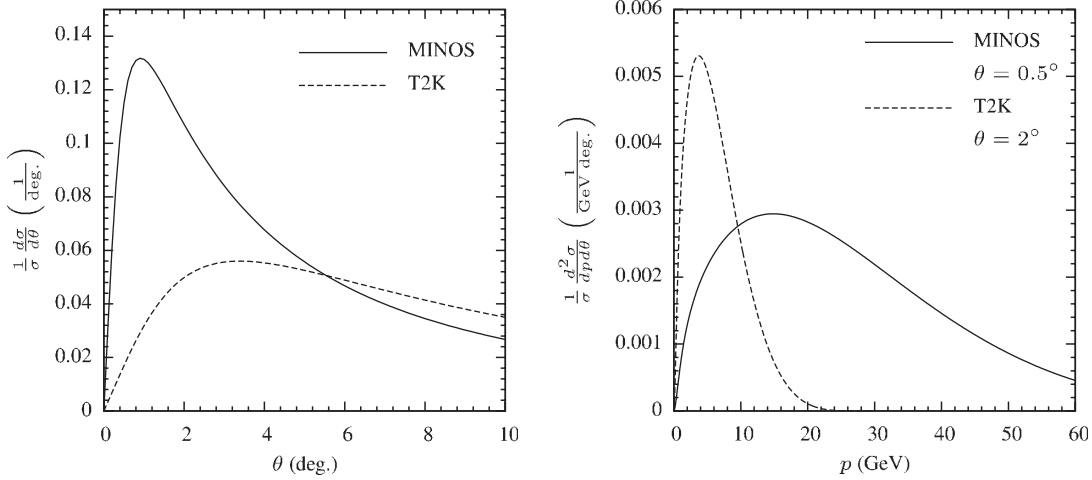
FIG. 6. Pseudoscalar meson production distributions $f^{\text{BMPT}}(\theta, p)$ in angle (left panel) and momentum (right panel), according to the fit [19], scaled to the beam energy and target composition for MINOS and T2K. These distributions determine the indirect production of vectors via, e.g., $\eta \to V\gamma$. Note that the fitted distributions have an unphysical low-energy tail at large angles which we exclude in the analysis.

scaling the NA61 measured total cross section using the relative magnitudes of the BMPT distributions for T2K and MINOS.[1] The production rates of negatively and positively charged pions are averaged, and differ by $\mathcal{O}(1)$ factors (see, e.g., Ref. [19]). To estimate the η production rate, we use this averaged distribution and make use of some early experimental data [21,22], which indicates that in the appropriate energy range

$$\sigma_{pp \to pp\pi} \approx (25\text{–}30)\sigma_{pp \to pp\eta}. \qquad (17)$$

This production mode is most relevant for V, and in the case $\phi = \pi^0$ or η the branching ratio to V is proportional to that of the radiative decay to two photons, though suppressed by coupling and phase space factors,

$$\mathrm{Br}_{\phi \to \gamma V} \simeq 2\kappa^2 \left(1 - \frac{m_V^2}{m_\phi^2}\right)^3 \mathrm{Br}_{\phi \to \gamma\gamma}. \qquad (18)$$

For η decays, as will be relevant here, $\mathrm{Br}_{\eta \to \gamma\gamma} \simeq 0.39$. This process becomes less competitive for larger mediator masses. We also explored the rate of V production due to radiative decays of $c\bar{c}$ mesons such as $J/\psi \to V\eta$, but the overall rate is well below that of direct production discussed above.

---

[1]The total π^+ flux could also be determined by working backwards from the measured neutrino flux, accounting for the angular acceptance of the detector [11]. However, this reconstruction is more complex when the majority of pions decay in flight and are affected by magnetic focusing horns.

After either direct or indirect production, the suppressed portal couplings ensure that the real or virtual X has an order-one branching to the hidden sector, $\mathrm{Br}_{X \to 2\chi} \simeq 1$. For completeness, we note that away from thresholds, the ratio of the decay rate of V to a single SM state [10] relative to the hidden sector is of order $\kappa^2 \alpha/\alpha'$, but is enhanced near resonances in hadronic channels and by the larger number of final states. In practice, $\mathrm{Br}(V \to \bar{\chi}\chi) = 1$ to a good approximation, apart from a small region near threshold of size $(1 - 4m_\chi^2/m_V^2)^n \lesssim \kappa^2 \alpha/\alpha'$ where the exponent $n = 1/2$ (fermionic χ) and $n = 3/2$ (scalar χ). We will excise this near-threshold region from the mass range.

The dark matter beam then propagates along with the neutrinos. For the couplings considered here, it has a weak-scale scattering rate with normal matter and is detectable through neutral current-like elastic scattering processes with electrons or, of most relevance here, with nucleons. We will utilize the parameters and data sets of MiniBooNE, MINOS and T2K to probe this scenario. Importantly, MiniBooNE has published an analysis on neutrino elastic scattering, which DM scattering will closely mimic, which allows some estimate of backgrounds and efficiencies. MINOS and T2K allow access to a higher mass range. We employed a simulation to determine the dark matter flux incident on the detector, which will be described in more detail in Sec. IV, after we have considered the viable model scenarios.

III. MODEL SCENARIOS

The preceding analysis is applicable to generic scenarios of hidden sector states, coupled through the vector and scalar portals. In this section, we will study more concrete

models of sub-GeV dark matter, where the mediator mass satisfies $m_X > 2m_\chi$, focusing on thermal relics for which the abundance provides a constraint on the annihilation cross section.

A. Constraints

The constraints that we will take into account include:

(i) *Relic abundance.*—If χ is a thermal relic, the WMAP constraint on the relic density $\Omega_{\rm DM}h^2 \sim 0.1 \sim (0.1\ {\rm pb})/\langle\sigma v\rangle_{\rm fo}$ constrains the annihilation cross section at freeze-out to be $\langle\sigma v\rangle_{\rm fo} \sim 1$ pb. Even if the hidden sector state does not provide the dominant contribution to dark matter, the overclosure constraint $\langle\sigma v\rangle_{\rm fo} \gtrsim 1$ pb applies more generally.

(ii) *Impact on the CMB.*—In order not to distort the CMB due to energy injection into the intergalactic medium through annihilation, there are again restrictions on the annihilation cross section that become particularly severe for light DM. The constraint takes the form $f(z)\langle\sigma v\rangle_{\rm CMB} \lesssim 0.1(m_{\rm DM}/{\rm GeV})$ pb, where $f(z)$ is a redshift-dependent efficiency factor which for low mass varies from $f \sim 0.2$ for pion to $f \sim 1$ for electron final states [23]. These limits essentially exclude a thermal relic below a few GeV with an abundance fixed via s-channel annihilation. Even for asymmetric DM, the requirement that the symmetric component annihilate away efficiently prior to decoupling leads to a lower bound on the annihilation rate of the same order [24]. This narrows down the field of viable models to those with (velocity-suppressed) annihilation since $v \sim 10^{-8}$ in this epoch. Other indirect signatures of annihilation in the galaxy (where $v \sim 10^{-3}$) are then necessarily suppressed as well.

(iii) *Visible decays.*—Focusing first on the vector portal, we note that models where V decays predominantly to the dark sector are less constrained than those in which V is metastable and decays mainly to the SM. For example, the fixed target constraints on dark forces via leptonic V decays [8,11] are avoided here for this reason as V decays promptly to the dark sector. However, there are constraints from high-luminosity colliders (particularly the B-factories in the case of GeV-scale vectors) which are sensitive to rare, but prompt, V decays to the SM. In comparison to dark force searches where in the appropriate mass range ${\rm Br}(V \to l^+l^-) \sim \mathcal{O}(1)$, this SM branching is suppressed here by an additional factor of $\mathcal{O}(\alpha\kappa^2/\alpha')$. A dedicated analysis for the Higgs-strahlung signature [10] was recently carried out at *BABAR* [25], leading to limits translating to $\kappa^4 \lesssim$ few $\times 10^{-7}$ in the present scenario. However, this only applies when the dark Higgs is heavy enough to decay predominantly to

two $V's$. Although there are no specific analyses, one can infer B-factory (and ϕ-factory) limits on generic continuum processes, $e^+e^- \to V^*\gamma \to l^+l^-\gamma$ (and any exclusive decays, e.g., of $\Upsilon(nS)$ or ϕ, not forbidden by C-parity [26]). The lack of significant peaks in similar rare-decay analyses suggests that limits, which in the present case translate to $(\alpha/\alpha')\kappa^4 \lesssim 10^{-6}$, apply more generally [6,9].

For the Higgs portal, there are significant B-factory limits on rare B decays, ${\rm Br}(B \to K + \not{E}) \lesssim 10^{-5}$, which directly constrain DM coupled via the Higgs portal [27] due to decays of the form $B \to K + \chi + \bar{\chi}$.

(iv) *Invisible decays.*—The scenarios considered here allow for the mediator to decay on-shell to dark matter, leading to new invisible decay channels [2,28,29]. Searches for rare radiative decays with missing energy, such as $J/\psi \to \gamma + \not{E}$ [30], are limited in the present case by C-parity but there are also generic limits on purely invisible decays of J/ψ and $\Upsilon(1S)$ [31] that constrain, e.g., $J/\psi \to V^* \to \chi\chi^\dagger$. Off-resonance, the limit is of order $\alpha'\kappa^2 \lesssim$ few $\times 10^{-4}$ [29], which is weaker than the visible decay constraint for $\alpha' \sim \alpha$ but becomes more significant for larger values of $\alpha' \sim 1$. Moving close to the resonance, where, e.g., $m_V \approx m_{J/\psi}$, the limit becomes particularly stringent, $\kappa^2/\alpha' \lesssim$ few $\times 10^{-6}$. However, since the V is still quite narrow for perturbative values of α', this only applies in a small V mass range, which for J/ψ and $\Upsilon(1S)$ decays is somewhat above the scale considered here. We note that future limits on invisible decays, e.g., of ϕ, would be sensitive to these scenarios.

(v) *Energy injection during big bang nucleosynthesis (BBN).*—Energy injection from decays of GeV-scale mediators in the early universe can be problematic if it occurs through hadronic channels before about 10^{-2} s. In the present case, most decays will occur to the hidden sector. Furthermore, the couplings are sufficiently large to ensure that decays occur well before BBN, so there are no significant constraints from this source.

(vi) *Self-interactions.*—The models we are considering here will become nonperturbative when the couplings exceed the naive dimensional analysis (NDA) scale of order $\alpha' \sim 4\pi$ (for the vector portal) and $\beta \sim 1$ (for the scalar portal). These rough limits characterize the point beyond which our perturbative analysis breaks down, with a transfer cross section of order $\sigma_{\rm trans} \sim 4\pi(\alpha')^2 m_\chi^2/m_X^4 \sim 10^{-25}$ cm^2 for a GeV-scale mediator. However, physical constraints on self-interaction are comparable in the low mass range. Limits on halo ellipticity generally require that the transfer cross section for scattering is below

about 10^{-23}–10^{-25} cm^2 [32]; some limits down to 10^{-26} cm^2 do appear in the literature (see Refs. [24,33] for recent discussions). This leads to similar limits on α' and β as the NDA limits quoted above.

B. Models and annihilation rates

In this subsection we briefly outline the parameter space for a couple of DM scenarios, with the above constraints in mind. We will focus on thermal WIMPs, so that the annihilation rate determines the relic density. With sub-GeV masses, there are stringent constraints on models with s-wave annihilation cross sections, so we will focus on the cases that are p-wave suppressed, namely scalar DM coupled to the vector portal and Majorana DM coupled to the scalar portal.

(i) *Scalar dark matter with a U(1) mediator.*—The model contains four parameters: the masses m_χ and m_V of the dark matter candidate and the vector mediator, the $U(1)'$ gauge coupling e', and the kinetic mixing coefficient κ. On requiring that χ comprises the majority of dark matter, the constraint on its relic abundance allows us to fix one relation between these four parameters. The primary quantity here is the annihilation rate, which for the GeV mass range of interest is given by s-channel diagrams with e^+e^-, $\mu^+\mu^-$, and light hadronic final states. In the limit of small mixing, we can approximate this rate by

$$\langle\sigma v\rangle_{\mathrm{ann,V}} \simeq \langle\sigma v\rangle_e + \langle\sigma v\rangle_\mu (1 + R(s = 4m_\chi^2)), \quad (19)$$

where $R = \sigma_{e^+e^- \to \mathrm{hadrons}}/\sigma_{e^+e^- \to \mu^+\mu^-}$, and the leptonic annihilation rate is [3]

$$\langle\sigma v\rangle_l = \frac{16\pi\kappa^2\alpha\alpha'}{3}\langle v^2\rangle$$
$$\times \frac{2m_\chi^2 + m_l^2}{(m_V^2 - 4m_\chi^2)^2 + m_V^2\Gamma_V^2}\sqrt{1 - \frac{m_l^2}{m_\chi^2}}. \quad (20)$$

For $m_\chi \ll m_V \sim 1$ GeV, this rate scales as $\langle\sigma v\rangle_l \sim 10^{-33}\kappa^2(\alpha'/\alpha)(m_\chi/100 \text{ MeV})^2 \text{ cm}^2$ using $v \sim 0.3$ at freeze-out. Accounting for all annihilation channels, the observed relic density $\Omega_{\mathrm{DM}}h^2 \sim 0.1 \sim (0.1 \text{ pb})/\langle\sigma v\rangle_{\mathrm{fo}}$ reduces the number of free parameters to three via a constraint that fixes $\alpha' = \alpha'(m_\chi, m_V, \kappa)$.

The p-wave suppression of annihilation for low velocities allows this process to satisfy the CMB constraints [23] alluded to above, as well as the galactic annihilation flux limits.

(ii) *Majorana dark matter with a scalar mediator.*—This model is a natural hidden sector generalization of the minimal model of scalar dark matter, and there are again four parameters: the masses m_χ and m_S, the hidden sector coupling β and the mixing angle θ. The abundance constraint will again allow us to determine, e.g., $\beta = \beta(m_\chi, m_S, \theta)$. Annihilation proceeds in the p-wave via mixing with the Higgs in the s-channel, and thus the rate is dictated by the light Higgs width. Given that $m_S \ll m_h$, the cross section scales as $\langle\sigma v\rangle_{\mathrm{ann,S}} \sim \beta^2\theta^2 m_\chi^2\langle v^2\rangle(\Gamma_{h^*}/m_{h^*})/(m_S^2 - 4m_\chi^2)^2$, where h^* refers to a virtual Higgs of mass $2m_\chi$. This rate is Yukawa-suppressed by the Higgs width Γ_{h^*} unless the Higgs mixing angle $\theta \sim Av/m_h^2$ and β are relatively large. However, these couplings are in turn constrained by the B-factory limits on rare B-decays with missing energy. The limits of [27] imply that $\beta^2\theta^2 m_\chi^2 v_{\mathrm{EW}}^2/m_S^4 \lesssim \mathcal{O}(1)$, which we see is quite stringent for mediator and DM masses in the GeV range. These B-decay limits make this scenario quite problematic as a model of thermal relic dark matter.

C. Summary

We can summarize the conclusions as follows for the four scenarios covered here:

(i) *Vector portal, scalar χ.*—This DM candidate exhibits p-wave annihilation, which is crucial to satisfy galactic and CMB annihilation limits, and thus is viable for subpercent mixing via the portal coupling. The sensitivity of neutrino facilities is significant in this case.

(ii) *Vector portal, fermionic χ.*—This implies s-wave annihilation, and the CMB annihilation limits can only be satisfied if χ is a highly subdominant component of WIMP dark matter, or has a more complex thermal history.

(iii) *Scalar portal, scalar χ.*—This again implies s-wave annihilation, suppressed in this case by the small Yukawa couplings. Thermal freeze-out would necessitate large mixing, which would rule out this scenario either due to the limits on rare B-decays, or its impact on the CMB.

(iv) *Scalar portal, fermionic χ.*—This DM candidate exhibits p-wave annihilation, which can avoid the CMB constraints, but to ensure the correct relic abundance the mixing must again be large, which is strongly constrained by rare B-decays.

Combining this information with the knowledge that DM coupled via the Higgs portal has a suppressed production rate, we conclude that rare B-decays provide a more sensitive probe of the Higgs portal than dark matter beams. However, scalar DM coupled via the vector portal is a viable model and we will focus on this scenario in the

next section, where we outline the sensitivity of neutrino facilities to a GeV-scale dark matter beam.

IV. SENSITIVITY TO A GEV DARK MATTER BEAM

A. Scattering

The detection strategy studied here uses elastic scattering of the DM beam in the (near-)detector. We outline

below the relevant cross sections, focusing on the vector mediator for the reasons discussed in the previous section.

(i) *Vector-mediated scattering.*—For a vector mediator, the scattering of scalar DM on nucleons shown in Fig. 7 is similar to neutrino-nucleon elastic scattering (see, e.g., Ref. [34]), and the cross section takes the form

$$\frac{d\sigma^V_{\chi N \to \chi N}}{dE_\chi} = \frac{\alpha' \kappa^2}{\alpha} \times \frac{4\pi\alpha^2[F^2_{1,N}(Q^2)A(E,E_\chi) - \frac{1}{4}F^2_{2,N}(Q^2)B(E,E_\chi)]}{(m^2_V + 2m_N(E - E_\chi))^2(E^2 - m^2_\chi)}, \tag{21}$$

where E and E_χ are the energies of the incident and outgoing dark matter particles, respectively, and $Q^2 = 2m_N(E - E_\chi)$ is the momentum transfer. We use simple monopole and dipole form-factors, $F_{1,N} = q_N/(1 + Q^2/m^2_N)^2$ and $F_{2,N} = \kappa_N/(1 + Q^2/m^2_N)^2$, where $q_p = 1$, $q_n = 0$, $\kappa_p = 1.79$ and $\kappa_n = -1.9$. The functions A and B are defined as

$$A(E, E_\chi) = 2m_N E E_\chi - m^2_\chi(E - E_\chi), \tag{22}$$

$$\begin{aligned} B(E, E_\chi) = (E_\chi - E)[(E_\chi + E)^2 \\ + 2m_N(E_\chi - E) - 4m^2_\chi]. \end{aligned} \tag{23}$$

(ii) *Scalar-mediated scattering.*—For a scalar mediator, the t-channel scattering cross section of Majorana fermion DM on nucleons takes a similar form to the monopole contribution to (21), but in place of $\kappa^2 \alpha \alpha'$ the cross section is suppressed by a factor $\beta^2 \theta^2 m^2_N f^2_{Ts}/v^2_{EW}$, where we have dropped isospin-violating corrections to the Higgs-nucleon coupling, and retained just the dominant contribution from $f_{Ts} \sim 0.118$ where $m_N f_{Tq} \equiv \langle N|m_q \bar{q}q|N \rangle$. Up to scalar mixing, this is analogous to conventional Higgs-mediated scattering and thus is quite suppressed relative the vector case above. Given the suppressed production rate, we will not consider this case further in this section.

To account for the isotopic content of the detector material, we will use an effective differential cross section, given by

$$\frac{d\sigma^{\text{eff}}_{\chi N}}{dE_f} \simeq \frac{Z}{A}\frac{d\sigma_{\chi p \to \chi p}}{dE_\chi} + \frac{A - Z}{A}\frac{d\sigma_{\chi n \to \chi n}}{dE_\chi}. \tag{24}$$

This expression is an approximation which ignores the differing detection efficiencies for scattering of bound nucleons. However, the Q^2-dependent efficiency factors quoted by MiniBooNE [18], for example, are close to one. Thus the error introduced by this simplification is small relative to the precision of our computation.

B. Simulation

A Monte Carlo simulation was employed to determine the kinematics of both the directly and indirectly produced dark matter beams. With the kinematics in hand, it is possible to calculate the expected sensitivity of MiniBooNE, MINOS and T2K to the hidden sector scenarios discussed in Sec. III, and the production channels of Sec. II. A detailed description of the simulation of the indirect production channel at MiniBooNE can be found in Ref. [12]. Some of the pertinent parameters for each experiment are listed in Table I, and we include some additional remarks below:

(i) *MINOS.*—The MINOS experiment utilizes 120 GeV protons from the NuMI beam line impacting a graphite target. The near-detector has a large overall mass, but only part of the cross sectional area of the detector is instrumented and the near-detector itself is nearly 1 km from the target. Nonetheless, the large boost provided by the 120 GeV proton beam leads to a significant event rate for dark matter scattering. We use an estimate for the total protons on target (POT) prior to the 2012 shutdown for the NOvA upgrade.

(ii) *T2K.*—The T2K experiment has only been operating since 2010, and rather than use the current data set we have taken into account the final number of POT expected for the current run. T2K utilizes a 30 GeV proton beam impacting a graphite target, and has two near detectors, ND280 and INGRID, both located in a complex 280 m from the target.

FIG. 7.　Tree-level dark matter scattering off nucleons mediated by the vector and scalar portals.

TABLE I. A summary of the parameters used for the three experiments considered in this work; see, e.g., Refs. [18,35–37] for MiniBooNE, [38–42] for MINOS, and [43–46] for T2K. Further details are in the text including a description of the notation. Note that in the absence of published analyses focusing on neutral currents, the overall efficiency ϵ_{eff} for T2K is not known; we take it to be of the same order as ϵ_{eff} for MINOS.

	Target	l_T	POT	E_{beam}	L	$A_{\text{det}}(\text{cm}^2)$	L_{det}	$n_N(\text{cm}^{-3})$	Fiducial mass	ϵ_{eff}
MiniBooNE	Be	71 cm	1.2×10^{21}	8.9 GeV	541 m	1.2×10^{6}	11.5 m	9×10^{23}	~650 tons	0.6
MINOS	C	94 cm	1.5×10^{21}	120 GeV	965 m	7.1×10^{4}	1.3 m	5×10^{24}	27 tons	0.8
T2K ND280	C	90 cm	5×10^{21}	30 GeV	280 m	5.5×10^{4}	0.7 m	4×10^{23}	1.67 tons	~
T2K INGRID	C	90 cm	5×10^{21}	30 GeV	280 m	2.2×10^{5}	0.585 m	5×10^{24}	~110 tons	~

ND280 is about 2 deg off-axis and is well-instrumented with time projection chambers for tracking and analysis, while INGRID is on-axis and contains significantly more fiducial mass.

(iii) *MiniBooNE.*—The MiniBooNE experiment utilizes an 8.9 GeV proton beam impacting a Germanium target and, distinct from MINOS and T2K, has a single spherical mineral oil detector located 541 m from the target. This detector has a large fiducial mass, and importantly MiniBooNE has already published a full neutrino elastic scattering analysis [18] with $\mathcal{O}(10^5)$ events and a measured energy spectrum, which provides the natural background for any dark matter beam search. We use an estimate for the total POT prior to the 2012 shutdown for the NOvA upgrade.

The simulation of the dark matter beam used a re-weighting technique, first determining the dark matter trajectories that intersect the detector, and subsequently weighting them according to the production distributions discussed earlier in Sec. II. We will describe these two steps in more detail below, starting with the generation of the dark matter trajectories.

For direct production at either T2K or MINOS, the V's were generated over an array of kinematically allowed momenta, and each V was decayed isotropically into a random pair of χ's in the V's center of mass frame. The lifetime of the V is short enough for the parameter space considered that it will decay before escaping the target, and so the propagation of the V through the target is ignored in the simulation. The trajectories of each of the χ particles are then checked to determine if they pass through the fiducial volume of the corresponding near detector. These trajectories are recorded along with the energy of the χ. The treatment of indirect production at T2K, MINOS and MiniBooNE was similar (see Ref. [12]), but required the extra initial step of first generating kinematically allowed meson trajectories, with each then decayed isotropically into a V and a γ in the meson rest frame. The newly produced V is then treated in the same manner as in the direct production simulation.

With the trajectories in hand, for each point in parameter space the expected number of events could be determined

by weighting them according to the production distribution $f(\theta, p)$, the scattering cross section $\sigma_{N\chi}^{\text{eff}}(E)$, and the distance R which χ propagates through the detector. There is also an overall measure factor: $\Delta = \delta p \delta \theta \delta \phi / (2\pi)$ for indirect production, or $\Delta = \delta p$ for direct production, where the δ quantities refer to the step sizes used in the simulation for ϕ or V production. Note that the distance R travelled through the MINOS near detector and ND280 will almost always equal the length of the detector L_{det} shown in Table I. For INGRID, it will occasionally be twice the listed number if it passes through the center of the detector, where two of the detector's modules overlap. MiniBooNE uses a spherical detector, and so R can vary significantly in this case.

The final expression for the expected number of elastic nucleon dark matter scattering events is given by

$$N_{N\chi \to N\chi} = n_N \times \epsilon_{\text{eff}}$$
$$\times \sum_{\text{prod. chan.}} \left(N_\chi \sum_{\text{trajec. } i} R_i \sigma_{N\chi}^{\text{eff}}(E_i) f(\theta_i, p_i) \Delta_i \right),$$
(25)

where n_N is the nucleon density in the detector, while ϵ_{eff} is the detection efficiency for events within the specified fiducial volume and cuts on momentum transfer. We will assume that lower cuts are above the range for coherent elastic scattering, so that our nucleon-level treatment in (24) should be reliable. We will also assume that the detection efficiencies do not deteriorate significantly for the full range of momentum transfer relevant for DM scattering. The production quantities are given by

$$N_\chi = \begin{cases} 2N_{\text{POT}} \times n_T l_T \sigma_{PT} & \text{direct} \\ 2N_\varphi \times \text{Br}(\varphi \to X + \cdots) & \text{indirect} \end{cases},$$
(26)

$$f(\theta, p) = \begin{cases} f_V(p) \times \frac{3}{4}(1 - \cos^2\theta) & \text{direct} \\ f_\varphi^{\text{IND}}(\theta, p) & \text{indirect} \end{cases}.$$
(27)

The distributions for direct $(f_V(p))$ and indirect $(f^{\text{IND}}(\theta, p) = f_\varphi^{\text{BMPT}}(\theta, p)$ or $f^{\text{SW}}(\theta, p))$ production were
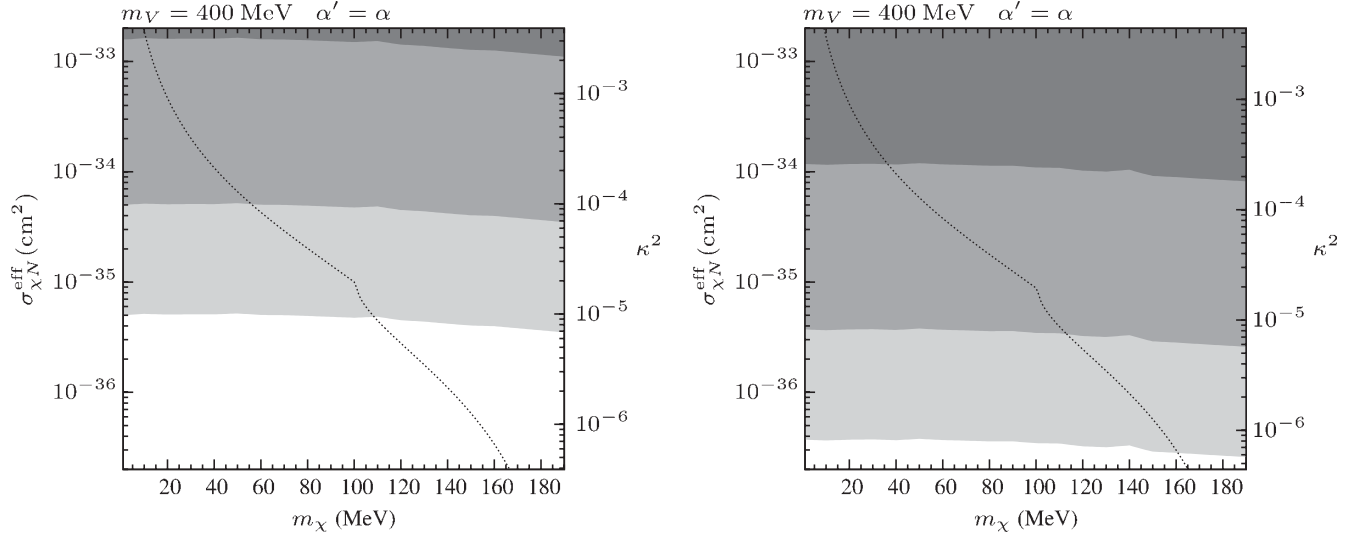
FIG. 8. Expected number of neutral currentlike dark matter nucleon scattering events from V's produced through η decays for the ND280 (left panel) and INGRID (right panel) detectors at T2K with $m_V = 400$ MeV. The regions show greater than 10 (light), 1000 (medium) and 10^6 (dark) expected events. The dashed curve indicates the value of κ required for the dark matter annihilation cross section in the early universe to equal 1 pb.
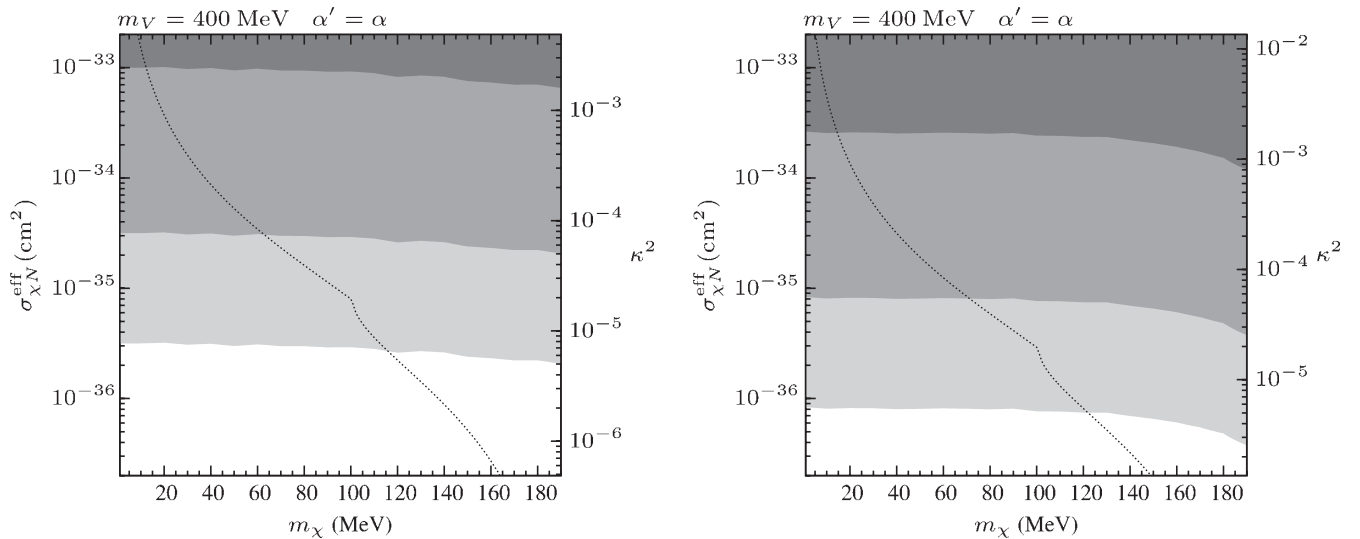
FIG. 9. Expected number of neutral currentlike dark matter nucleon scattering events from V's produced through η decays for the MINOS near detector (left panel) and MiniBooNE (right panel) with $m_V = 400$ MeV. The contours are described in Fig. 8.

discussed in Sec. II.[2] Note that the meaning of p and θ varies depending on the context. For direct production, p is the V momentum, and θ is the angle between the dark matter and the beam in the V rest frame. For indirect production, both p and θ refer to those of the original meson ϕ in the lab frame. The direct production parameters in N_χ are the number of protons on target N_{POT}, the

target length l_T and density n_T, and the total cross section σ_{PT}. The experimental quantities are listed in Table I, while our treatment of σ_{PT} was discussed in Sec. II. For indirect production, we use an estimate of the total $\phi = \eta$ yield N_η and the branching ratio to the mediator.

C. Results

The results for DM nucleon scattering at MINOS, T2K, and MiniBooNE are shown for various parameter choices in Figs. 8–13. All the plots show contours of the number of events (10, 1000, or 10^6) in the plane of nucleon scattering

---

[2]For T2K, rather than $f^{\mathrm{BMPT}}(\theta, p)$, the indirect production distribution used was a parametrization of data from NA61 [20], using a replica T2K target. However, the results are consistent with those using the BMPT parametrization.
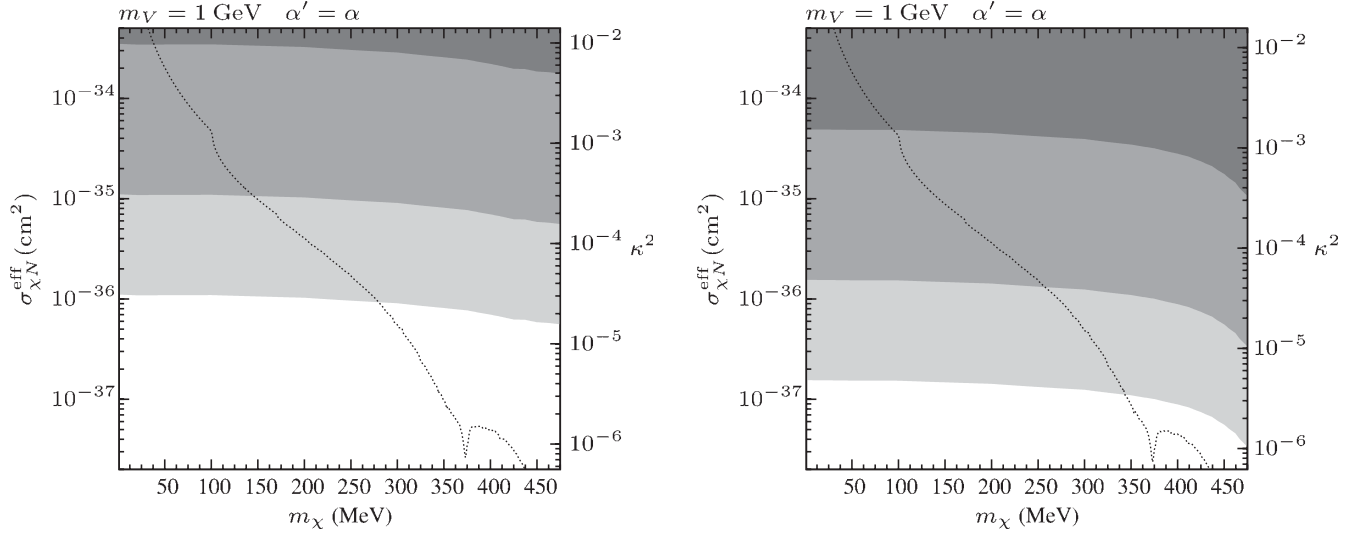
FIG. 10. Expected number of neutral currentlike dark matter nucleon scattering events from direct V production for the ND280 (left panel) and INGRID (right panel) detectors at T2K with $m_V = 1$ GeV. The contours are described in Fig. 8.

cross section (or kinetic mixing κ^2) versus dark matter mass. The sensitivity tends to be fairly flat as a function of m_χ, as the momentum transfer in the scattering tends to be much larger than the mass and thus m_χ drops out of the kinematics. The exception to this general rule is that when m_χ approaches the decay threshold, $m_\chi \sim m_V/2$, there is an enhancement in sensitivity as the dark matter has a small transverse boost from the V decay and thus a larger fraction of trajectories will intersect on-axis detectors. The overlaid dark line denotes the parameter choices consistent with χ having the correct thermal relic density to form WIMP dark matter. The structure in this curve for higher mass reflects the ρ/ω and ϕ hadronic resonances that play a role in annihilation. Note that the position of the

thresholds and resonances is shifted down slightly from $2m_\chi$ due to the kinetic energy of the WIMPs. Assuming an initial thermal abundance, the WIMP relic density would be too large in regions of parameter space below this curve.

Existing particle physics limits on the parameter space would, as discussed in Sec. III, require that κ and α' satisfy both $(\alpha/\alpha')\kappa^4 \lesssim 10^{-6}$ and $\alpha'\kappa^2 \lesssim$ few $\times 10^{-4}$ for models of this type. For the perturbative values of $\alpha' \sim \alpha$ that will primarily be used in what follows, the former limit is more restrictive implying $\kappa^2 \lesssim 10^{-3}$. However, this constraint is inferred from B-factory analyses of somewhat different models rather than dedicated searches, so we refrain from showing any explicit exclusion curves. Nonetheless, with this benchmark in mind we observe
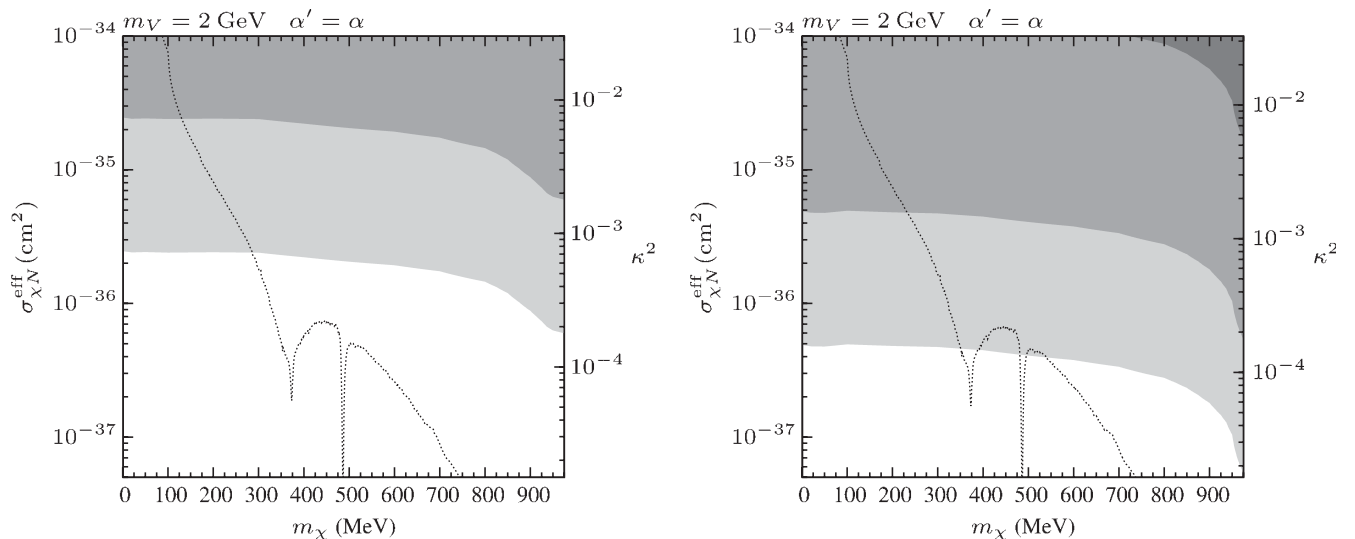
FIG. 11. Expected number of neutral currentlike dark matter nucleon scattering events from direct V production for the ND280 (left panel) and INGRID (right panel) detectors at T2K with $m_V = 2$ GeV. The contours are described in Fig. 8.
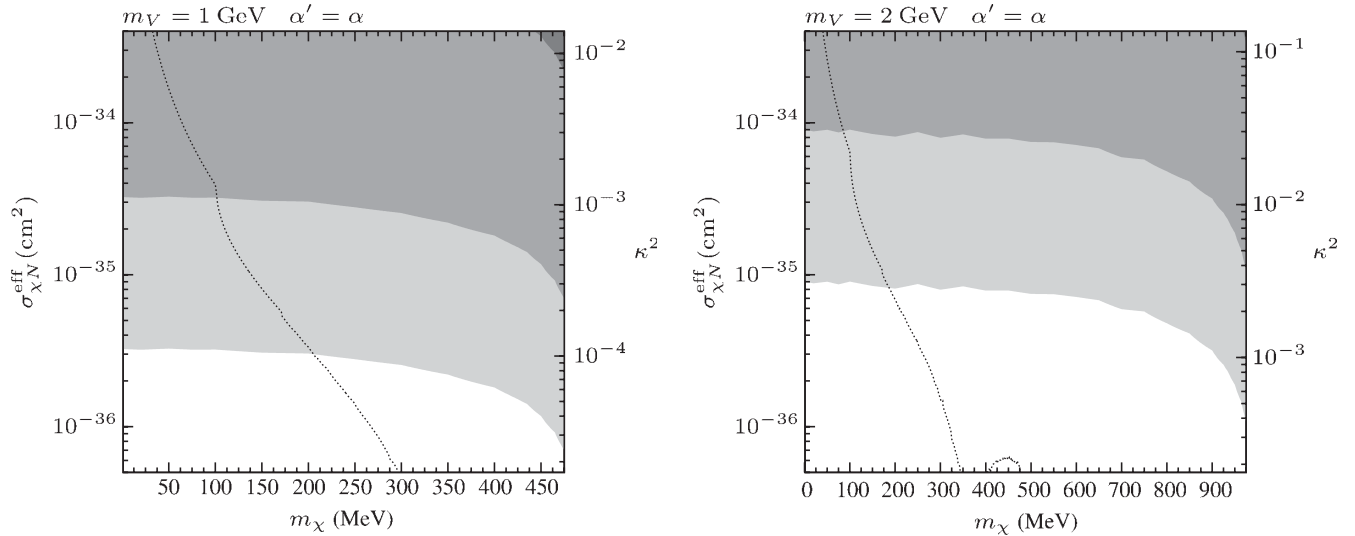
FIG. 12.   Expected number of neutral currentlike dark matter nucleon scattering events through direct V production for the MINOS near detector with two different vector mediator masses ($m_V = 1$ GeV on the left and $m_V = 2$ GeV on the right). The contours are described in Fig. 8.

from the plots that interesting sensitivity emerges with the ability to distinguish $\mathcal{O}(10^3–10^4)$ dark matter scattering events from the neutrino background. The characteristic scattering cross section per nucleon to achieve $\mathcal{O}(1000)$ events ranges from 1–10 pb, which is an impressive level of sensitivity. Since this is not coherent scattering, it is more useful to contrast it with the best low mass sensitivity achieved for spin-dependent scattering in underground detectors [47] which is around 0.1 pb for $m_\chi \sim 10$ GeV, but drops off rapidly for lower masses. Of course, to implement a search for $\mathcal{O}(1000)$ events would require the ability to separate this from the neutrino background of

$\mathcal{O}(10^5–10^6)$ events. We will comment further on possible search strategies and means for background rejection in the next section.

The individual plots reveal a number of other features summarized below:

(i) In Figs. 8 and 9 we exhibit the sensitivity to dark matter in the 100–200 MeV mass range, with $m_V = 400$ MeV. The direct parton-level approximation for on-shell production of such low-mass vectors is questionable with the PDF scale set to $Q = m_V$, so we use indirect production via η-decays. As there is no significant resonant enhancement in η
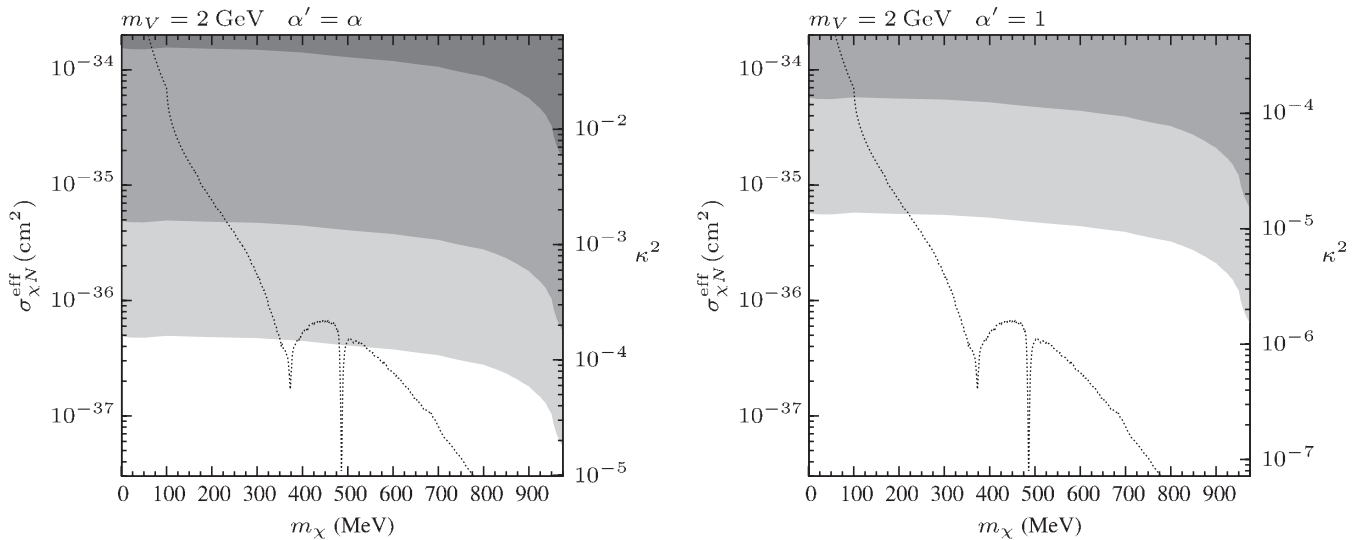
FIG. 13.   Expected number of neutral currentlike dark matter nucleon scattering events from direct V production with the INGRID detector at T2K, comparing two different α values ($\alpha' = \alpha$ on the left and $\alpha' = 1$ on the right) for a 2 GeV Vector mediator. The contours are described in Fig. 8.

production, one should bear in mind that this may be an underestimate for total V-production in this mass range. The ensuing sensitivity is shown for T2K in Fig. 8, and for MiniBooNE and MINOS in Fig. 9. Note that the lower momentum transfer in scattering at MiniBooNE leads to an enhanced sensitivity to the cross section for a given sensitivity in κ, relative to MINOS.

(ii) In Figs. 10 and 11 for T2K and Fig. 12 for MINOS we exhibit the sensitivity to higher-mass dark matter, for $m_V = 1$ and 2 GeV using direct parton-level production. We expect the narrow width approximation to work fairly well for 2 GeV vectors with this mass setting the PDF scale. The precision of the estimate will certainly be lower using this method for 1 GeV vectors, due to the uncertainties in the PDFs and the importance of higher-order QCD corrections. Nonetheless, we see that the tree-level sensitivity for 1 GeV vectors is only marginally enhanced relative to $m_V = 2$ GeV.

(iii) Using Figs. 10 and 11, it is interesting to compare the sensitivity of the two near-detectors at T2K. Given the suppression of direct χ-production in the forward direction, the off-axis ND280 detector at T2K is ideally positioned to capture a comparatively large flux of dark matter, as compared to the on-axis detector INGRID. However, the much larger active mass of INGRID more than counteracts this effect, leading to an enhanced sensitivity. We are not aware if T2K has plans to use INGRID for analyses unrelated to diagnostics of the neutrino beam, but we see that there is considerable intrinsic sensitivity to light dark matter.

(iv) In Fig. 13 we compare the direct production sensitivity of the INGRID detector at T2K for two values of the dark U(1) coupling $\alpha' = \alpha$ and $\alpha' = 1$. The latter value implies a self-interaction cross section for dark matter $\sigma \sim 4\pi m_\chi^2/m_V^4$ that can reach $\mathcal{O}(0.1 \text{ mb})$ for a 1 GeV mediator. This is close to, but somewhat below, the scale that would lead to detectable effects on halo structure, which may be relevant to the understanding of the inner regions of dwarf spheroidal halos. As is apparent from the plot, increasing α' has the effect of enhancing the annihilation rate and thus moving the relic density curve to lower values of κ. Consequently, this increases the intrinsic sensitivity to κ while effectively lowering the sensitivity to the scattering cross section. Analogous sensitivity to α' applies to the other parameter regimes and experiments shown in the earlier plots which all assume $\alpha' = \alpha$.

(v) The plots all indicate that very light WIMPs with masses below about 100 MeV are problematic as thermal relics. Even for larger values of α', the event rate along the measured relic density curve grows as m_χ decreases, and reaches levels which are well above the elastic scattering rate for neutrinos. Thus, the measured elastic scattering of neutrinos at these facilities, and its consistency with the standard model, serves to exclude a large class of models of MeV scale dark matter. This strong tension with models of MeV-scale dark matter was already exhibited in more detail using data from LSND and MiniBooNE in Ref. [12].

V. CONCLUDING REMARKS

The direct search for dark matter is above all a search for weakly interacting degrees of freedom, and at this stage the mass range is relatively unconstrained. The LHC has as yet revealed little sign of new weak-scale physics, so it is important to keep in mind that the simple thermal relic paradigm is broad enough to encompass a large mass range, extending well below the weak scale. Thus it is crucial to utilize all the available experimental tools to explore the viable dark matter parameter space. The weak nature of DM–SM interactions means that fixed target neutrino experiments provide a very natural source of low mass sensitivity. This goes both ways, as the next generation of underground dark matter direct detection experiments may in turn be able to detect various astrophysical and cosmological sources of neutrinos. Rather than being simply an irreducible background, it seems clear that these experiments will have to become observatories for all types of cosmic weakly interacting degrees of freedom. In this paper, we have explored another aspect of this convergence, namely the use of neutrino beam experiments to probe light dark matter that can be produced in the target, and undergo elastic scattering in the detector.

The challenge in developing a search strategy for this dark matter signal will be in disentangling the event spectrum from the neutrino background at a level of maybe 1–10%. This would allow sensitivity to kinetic mixing in the $\kappa^2 \lesssim 10^{-4}$–$10^{-5}$ range, which is the most viable regime given the level of indirect constraints. This level of sensitivity to sub-GeV WIMPs, at the pb level in terms of per-nucleon scattering cross section, is only attained in spin-dependent direct detection for WIMPs with much larger masses, exceeding 10 GeV. Thus neutrino experiments could provide an important means of probing dark matter nucleon scattering below the mass range accessible via direct detection. In terms of isolating dark matter beam scattering events from the large background of neutrino elastic scattering, we note that there are several distinctive characteristics. Firstly, the dark matter beam has a higher average energy (shown in Fig. 5) than the neutrino beam, and in particular a much higher cutoff that approaches the energy of the primary proton beam. This would permit a relatively high cut in momentum transfer in scattering, provided such events are retained in the full sample.

Secondly, the dark matter beam will be relatively unaffected by turning off or switching the polarity of the magnetic focusing horns, which would alter the neutrino beam significantly. Finally, there may also be useful information in the (nanosecond-scale) timing structure as the production mechanisms for vector-portal-coupled DM and the neutrino beam are quite distinct. Determining whether one or more of these features could be put to practical use in a search strategy would require a dedicated analysis.

In concluding, we would also like to comment on some alternative approaches to explore the light WIMP regime.

(i) Direct detection in the low mass range could be feasible using electron scattering, as explored in recent work [48]. This approach is quite complementary to the neutrino beam analysis considered here. While the beam analysis requires relatively heavy vectors with $m_V > 2m_\chi$, the sensitivity for electron scattering is enhanced when $m_V \ll m_\chi$. For comparison, the projected electron scattering sensitivity to the vector portal model considered here is relatively weak for $m_V \sim 1$ GeV, but becomes significant for $m_V \sim 1$ MeV [48]. Future progress using Ge crystals seems promising and may allow strong sensitivity to sub-GeV WIMPs with very light MeV-scale mediators, provided techniques are available to deal with all the backgrounds at such low recoil energies.

(ii) Direct collider searches are also possible, utilizing missing energy signatures such as monophotons or monojets [49]. However, the sensitivity weakens significantly with light mediators. Collider searches can also pursue signatures of the light mediators directly, e.g., via subleading SM decays which may produce signatures such as lepton jets at high energy. In the scenarios considered here, the decays of the mediator are all prompt so there are no displaced vertices.

Looking to the future, the continued development of long-baseline neutrino facilities provides an ideal setting for expanding the search for light hidden sector states. This sensitivity extends beyond the models of light dark matter discussed here to other classes of new physics, such as the scenarios discussed in Ref. [50], that could impact the neutrino sector more directly.

[1] C. Boehm, D. Hooper, J. Silk, M. Casse, and J. Paul, Phys. Rev. Lett. **92**, 101301 (2004); P. Gondolo and G. Gelmini, Phys. Rev. D **71**, 123520 (2005); D. P. Finkbeiner and N. Weiner, *ibid.* **76**, 083519 (2007); D. Hooper and K. M. Zurek, *ibid.* **77**, 087302 (2008); N. Arkani-Hamed, D. P. Finkbeiner, T. R. Slatyer, and N. Weiner, *ibid.* **79**, 015014 (2009); M. Pospelov and A. Ritz, Phys. Lett. B **671**, 391 (2009).

[2] P. Fayet, Phys. Rev. D **70**, 023514 (2004); **74**, 054034 (2006); **75**, 115017 (2007).

[3] C. Boehm and P. Fayet, Nucl. Phys. **B683**, 219 (2004).

[4] M. Pospelov, A. Ritz, and M. B. Voloshin, Phys. Lett. B **662**, 53 (2008).

[5] B. W. Lee and S. Weinberg, Phys. Rev. Lett. **39**, 165 (1977).

[6] N. Borodatchenkova, D. Choudhury, and M. Drees, Phys. Rev. Lett. **96**, 141802 (2006).

[7] M. Pospelov, Phys. Rev. D **80**, 095002 (2009).

[8] J. D. Bjorken, R. Essig, P. Schuster, and N. Toro, Phys. Rev. D **80**, 075018 (2009); P. Schuster, N. Toro, and I. Yavin, Phys. Rev. D **81**, 016002 (2010); R. Essig, P. Schuster, N. Toro, and B. Wojtsekhowski, J. High Energy Phys. 02 (2011) 009; R. Essig, R. Harnik, J. Kaplan, and N. Toro, Phys. Rev. D **82**, 113008 (2010).

[9] R. Essig, P. Schuster, and N. Toro, Phys. Rev. D **80**, 015003 (2009), http://arxiv.org/abs/0903.3941; M. Reece and L.-T. Wang, J. High Energy Phys. 07 (2009) 051.

[10] B. Batell, M. Pospelov, and A. Ritz, Phys. Rev. D **79**, 115008 (2009).

[11] B. Batell, M. Pospelov, and A. Ritz, Phys. Rev. D **80**, 095024 (2009).

[12] P. deNiverville, M. Pospelov, and A. Ritz, Phys. Rev. D **84**, 075020 (2011).

[13] L. J. Rosenberg and K. A. van Bibber, Phys. Rep. **325**, 1 (2000); G. Carosi and K. van Bibber, Lect. Notes Phys. **741**, 135 (2008); E. Gallas *et al.* (FMMF Collaboration), Phys. Rev. D **52**, 6 (1995); G. Bernardi, G. Carugno, J. Chauveau, F. Dicarlo, M. Dris *et al.*, Phys. Lett. B **203**, 332 (1988); J. Adams *et al.* (KTeV Collaboration), Phys. Rev. Lett. **79**, 4083 (1997); J. Badier *et al.* (NA3 Collaboration), Z. Phys. C **31**, 21 (1986); J. LoSecco, L. Sulak, R. Galik, J. Horstkotte, J. Knauer, H. H. Williams, A. Soukas, P. Wanderer, and W. Weng, Phys. Lett. **102B**, 209 (1981).

[14] R. Foot, H. Lew, and R. Volkas, Phys. Lett. B **272**, 67 (1991); R. Foot and X.-G. He, Phys. Lett. B **267**, 509 (1991).

[15] B. Patt and F. Wilczek, arXiv:hep-ph/0605188; R. Schabinger and J. D. Wells, Phys. Rev. D **72**, 093007 (2005); D. G. Cerdeno, A. Dedes, and T. E. J. Underwood, J. High Energy Phys. 09 (2006) 067; J. R. Espinosa and M. Quiros, Phys. Rev. D **76**, 076004 (2007); J. March-Russell, S. M. West, D. Cumberbatch, and D. Hooper, J. High Energy Phys. 07 (2008) 058; M. Ahlers, J. Jaeckel, J. Redondo, and A. Ringwald, Phys. Rev. D **78**, 075005 (2008); J. L. Feng, H. Tu, and H.-B. Yu, J. Cosmol. Astropart. Phys. 10 (2008) 043; K. Kohri, J. McDonald,

and N. Sahu, Phys. Rev. D **81**, 023530 (2010); J. L. Feng, M. Kaplinghat, H. Tu, and H.-B. Yu, J. Cosmol. Astropart. Phys. 07 (2009) 004.

[16] P. M. Nadolsky, H.-L. Lai, Q.-H. Cao, J. Huston, J. Pumplin, D. Stump, W.-K. Tung, and C.-P. Yuan, Phys. Rev. D **78**, 013004 (2008).

[17] H. M. Georgi, S. L. Glashow, M. E. Machacek, and D. V. Nanopoulos, Phys. Rev. Lett. **40**, 692 (1978).

[18] A. Aguilar-Arevalo *et al.* (MiniBooNE Collaboration), Phys. Rev. D **82**, 092005 (2010).

[19] M. Bonesini, A. Marchionni, F. Pietropaolo, and T. Tabarelli de Fatis, Eur. Phys. J. C **20**, 13 (2001).

[20] N. Abgrall *et al.* (NA61/SHINE Collaboration), Phys. Rev. C **84**, 034604 (2011).

[21] S. Teis, W. Cassing, M. Effenberger, A. Hombach, U. Mosel, and G. Wolf, Z. Phys. A **356**, 421 (1997).

[22] V. Flaminio, W. Moorhead, D. R. Morrison, and N. Rivoire, Report No. CERN-HERA-84-01.

[23] N. Padmanabhan and D. P. Finkbeiner, Phys. Rev. D **72**, 023508 (2005); T. R. Slatyer, N. Padmanabhan, and D. P. Finkbeiner, Phys. Rev. D **80**, 043526 (2009); S. Galli, F. Iocco, G. Bertone, and A. Melchiorri, Phys. Rev. D **84**, 027302 (2011); D. P. Finkbeiner, S. Galli, T. Lin, and T. R. Slatyer, Phys. Rev. D **85**, 043522 (2012).

[24] T. Lin, H.-B. Yu, and K. M. Zurek, Phys. Rev. D **85**, 063503 (2012).

[25] J. Lees *et al.* (*BABAR* Collaboration), Phys. Rev. Lett. **108**, 211801 (2012).

[26] B. Aubert *et al.* (*BABAR* Collaboration), arXiv:0902.2176; F. Archilli *et al.*, J. Phys. Conf. Ser. **335**, 012067 (2011).

[27] C. Bird, R. V. Kowalewski, and M. Pospelov, Mod. Phys. Lett. A **21**, 457 (2006).

[28] B. McElrath, Phys. Rev. D **72**, 103508 (2005).

[29] P. Fayet, Phys. Rev. D **81**, 054025 (2010).

[30] J. Insler *et al.* (CLEO Collaboration), Phys. Rev. D **81**, 091101 (2010).

[31] K. Nakamura *et al.* (Particle Data Group), J. Phys. G **37**, 075021 (2010).

[32] R. Dave, D. N. Spergel, P. J. Steinhardt, and B. D. Wandelt, Astrophys. J. **547**, 574 (2001).

[33] J. L. Feng, M. Kaplinghat, H. Tu, and H.-B. Yu, J. Cosmol. Astropart. Phys. 07 (2009) 004.

[34] L. Ahrens, S. Aronson, P. Connolly, B. Gibbard, M. Murtagh *et al.*, Phys. Rev. D **35**, 785 (1987).

[35] A. Aguilar-Arevalo *et al.* (MiniBooNE Collaboration), Phys. Rev. D **79**, 072002 (2009).

[36] D. Perevalov, Ph.D. thesis, University of Alabama, 2009.

[37] G. Karagiorgi (MiniBooNE Collaboration), *Appearance Results from MiniBooNE*, WIN 2012, http://www-boone.fnal.gov/slides-talks/conf-talk/georgiak/WIN11_miniboone.pdf.

[38] R. Pittam, fermilab-thesis-2010-43.

[39] P. Adamson *et al.* (MINOS Collaboration), Phys. Rev. Lett. **107**, 011802 (2011).

[40] P. Adamson *et al.* (MINOS Collaboration), Phys. Rev. D **81**, 052004 (2010).

[41] I. Ambats *et al.* (MINOS Collaboration), Report No. NUMI-L-337.

[42] M. Messier (MINOS Collaboration), *MINOS, NOvA, Fermilab Perspective*, http://nova-docdb.fnal.gov/cgi-bin/ShowDocument?docid=7197.

[43] K. Abe *et al.* (T2K Collaboration), Nucl. Instrum. Methods Phys. Res., Sect. A **659**, 106 (2011).

[44] F. de Blaszczyk, *T2K off-axis near detector ν_μ flux measurement and absolute momentum scale calibration of the off-axis near detector tracker*, http://www.t2k.org/docs/thesis/012.

[45] K. Abe, N. Abgrall, Y. Ajima, H. Aihara, J. Albert *et al.*, arXiv:1111.3119.

[46] T. Le (T2K Collaboration), arXiv:0910.4211.

[47] E. Behnke, J. Behnke, S. J. Brice, D. Broemmelsiek, J. I. Collar *et al.*, arXiv:1204.3094.

[48] R. Essig, J. Mardon, and T. Volansky, Phys. Rev. D **85**, 076007 (2012); P. W. Graham, D. E. Kaplan, S. Rajendran, and M. T. Walters, arXiv:1203.2531.

[49] J. Goodman, M. Ibe, A. Rajaraman, W. Shepherd, T. M. P. Tait, and H.-B. Yu , Phys. Rev. D **82**, 116010 (2010); P. J. Fox, R. Harnik, J. Kopp, and Y. Tsai, Phys. Rev. D **84**, 014028 (2011); A. Rajaraman, W. Shepherd, T. M. Tait, and A. M. Wijangco, Phys. Rev. D **84**, 095013 (2011); P. J. Fox, R. Harnik, J. Kopp, and Y. Tsai, Phys. Rev. D **85**, 056011 (2012); I. M. Shoemaker and L. Vecchi, arXiv:1112.5457.

[50] M. Pospelov, Phys. Rev. D **84**, 085008 (2011); M. Pospelov and J. Pradler, Phys. Rev. D **85**, 113016 (2012).